Facile synthesis of polydopamine/reduced graphene oxide nanosheets with incorporated copper ions for high antibacterial performance

Aiying Guo[1], *Yanfeng Sun*[2], *Xiaoyue Xu*[1], *Xiumin Yu*[1], *Xiaojie Wu*[1], *Aijun Cai*[1] ✉, *Ling Qin*[3]

[1]*College of Agronomy and Biotechnology, Hebei Normal University of Science & Technology, Qinhuangdao 066004, People's Republic of China*
[2]*Ocean College, Agricultural University of Hebei, Qinhuangdao 066003, People's Republic of China*
[3]*College of Bioscience and Bioengineering, Hebei University of Science and Technology, Shijiazhuang 050018, People's Republic of China*
✉ *E-mail: caiaijun80@163.com*

Published in Micro & Nano Letters; Received on 1st September 2019; Accepted on 11th November 2019

In this work, a facile and green approach for the synthesis of polydopamine/reduced graphene oxide nanosheets with incorporated copper ions (Cu/PDA/RGO) has been reported using bioadhesive PDA. During the process, the coating of PDA occurred through self-assembly and oxidative polymerisation, involving both the reduction of GO nanosheets and immobilisation of Cu ions. The Cu/PDA/RGO nanosheets showed effective and efficient antibacterial performance against *Escherichia coli* (*E. coli*) and *Staphylococcus aureus* (*S. aureus*). The antibacterial mechanism of the Cu/PDA/RGO nanosheets was also investigated. The death of *E. coli* cells could be attributed to the disruption of their cell membranes and increased levels of intracellular reactive oxygen species (ROS). However, due to the direct contact between the Cu/PDA/RGO nanosheets and cells, the production of high level ROS ultimately led to the death of *S. aureus* cells. This research provides a new idea for the synthesis of antibacterial agents.

1. Introduction: A steady increase in population has led to the destruction of the natural environment. Air and water contaminated by pathogenic microorganisms spread infectious diseases [1]. Although antibiotics can effectively cure infectious diseases, extensive use of antibiotics has resulted in new problems, such as the emergence of drug resistant pathogens (or multi-drug resistant pathogens) [2, 3] and superbugs [4, 5] posing more serious healthcare challenges [6, 7]. There is an urgent need to develop novel and effective antibacterial agents to tackle the problem of drug resistant bacteria [8]. Nowadays, large numbers of nanocomposites, such as metal oxides and metal nanoparticles (NPs) have shown excellent antibacterial properties [9–11]. They can kill microbes or inhibit their growth by destroying their cell membranes [11] or by increasing the level of reactive oxygen species (ROS). These nanomaterial-based compounds provide a new method to treat infectious diseases.

Among these metallic compounds, copper (Cu)-based NPs have shown great potential in disinfection of microorganisms and viruses [12, 13], since they are economical and biologically safe [9, 14–17]. Copper NPs (Cu NPs) have been synthesised by different methods, such as ultraviolet (UV)-light irradiation [15], co-precipitation method [17], chemical reduction [14, 18, 19], and biotemplated synthesis [16]. In these examples, generally, Cu salts (such as $CuSO_4$, $CuCl_2$, $Cu(NO_3)_2$) were used as precursors to obtain Cu NPs. However, most of these approaches required longer time, special equipment, toxic materials or more complicated procedures, and so on. Therefore, a simple, effective, and green method to synthesise Cu-based NPs remains a challenge.

Dopamine is widely used as a biogenic material [20] and it can self-polymerise in an alkaline medium. It can also spontaneously form a thin polydopamine (PDA) layer virtually on any surface. PDA coating not only has reducing properties but also serves as a versatile platform for secondary functionalisation of materials [21]. Graphene oxide (GO) coated with PDA has attracted great attention due to its excellent mechanical properties, large specific surface area and thermal and electrical properties [22, 23]. For example, according to Guo *et al.*, the reduction of noble metal (Au, Ag, Pt) on the surfaces of reduced GO (RGO) by PDA required 30 min to 5 h [24]. Hu *et al.* reported that PDA functionalised graphene sheets dispersed in $CuCl_2$ solution for 2 h produced rG–Cu, which could degrade methylene blue [25]. Yeroslavsky *et al.* synthesised Cu-containing PDA capsules by overnight refrigeration [26], which showed strong and rapid antibacterial activity. From these studies the advantages of PDA-based chemical modification technology, such as ease-of-use, environment-friendliness, and versatility under mild conditions, can be seen.

Inspired by these characteristics of PDA, dopamine was used in this study to reduce GO. The PDA coating obtained subsequently served as a platform for immobilisation of Cu ions. To the best of our knowledge, this is the first report on the deposition of Cu-based NPs on the surface of PDA/RGO to achieve antibacterial efficiency. In this study, the synthesis of Cu-based NPs required only 8 h and was carried out without using any other reducing agent. The process is very facile, efficient, and green. Antibacterial tests revealed that Cu/PDA/RGO nanosheets had efficient antibacterial performance against *Escherichia coli* (*E. coli*) and *Staphylococcus aureus* (*S. aureus*).

2. Materials and methods: Graphene powders were purchased from Sigma-Aldrich. Dopamine hydrochloride was obtained by Adramas Reagent Co., Ltd. *E. coli* (ATCC 25922) and *S. aureus* (ATCC 25923) were purchased from China Center of Industrial Culture Collection (Beijing, China). ROS assay kit was obtained from Beyotime Company (Beijing, China). Tris(hydroxymethyl) aminomethane, $CuSO_4$, acetone, glutaraldehyde, and Lysogeny broth (LB) medium were acquired from Tianjin Yong Da Chemical Reagent Development Center. Analytical grade chemicals were used without further purification. All solutions were prepared in deionised (DI) water purified using a Milli-Q ultrapure unit.

2.1. Synthesis of Cu/PDA/RGO nanosheets: GO was prepared according to the procedure described by Wang's team [27]. Then the Cu/PDA/RGO nanosheets were typically synthesised as follows: 200 mg GO was dispersed in 200 ml DI water, and the resulting suspension was sonicated in an ice-bath for 1.5 h.

doi: 10.1049/mnl.2019.0524

Then 200 mg dopamine hydrochloride and 200 ml Tris-buffer solution (10 mM, pH 8.5) were added to the above suspension and subsequently stirred for 12 h at room temperature to obtain the composites of reduced GO (PDA/RGO). The PDA/RGO composite was collected by centrifugation, followed by washing with DI water. Subsequently, the obtained PDA/RGO was re-dispersed in 200 ml DI water. After adding 500 mg $CuSO_4$, the suspension was stirred for 8 h. Finally, the as-prepared Cu/PDA/RGO nanosheets were separated by centrifugation and dried in an oven.

2.2. Characterisations: The crystal structure analysis was carried out on X-ray diffraction (XRD) measurement (Germany Bruker D8-ADVANCE, Cu-*kα* radiation). The surface morphology of the samples was examined using a transmission electron microscope (TEM, Dimension D3100, Veeco). The chemical components were characterised using X-ray photoelectron spectroscopy (XPS, Thermo VG Scientific). The total content of Cu in product was measured by inductively coupled plasma-optical emission spectrophotometry (ICP-OES, Perkin-Elmer Optima 2100).

2.3. Bacterial cells preparation: *E. coli* and *S. aureus* were chosen as model Gram-negative and Gram-positive bacteria, respectively, to investigate the antimicrobial properties of samples. Both stains were grown in LB medium at 37°C overnight, and then the cells were collected by centrifugation and washed several times with sterile DI water. Finally, the cells were adjusted to about 10^7–10^8 colony forming units (CFU)/ml for antibacterial assay.

2.4. Optical density (OD) growth curve determination: Cells suspension (2 ml) and samples (200 µl) of different concentrations (0, 40, 80, 120, 160, 200 µg/ml) were mixed and incubated at 37°C with shaking for 2 h. The mixture was then transferred into a 100 ml flask containing 20 ml of LB medium. The cell samples were incubated at 37°C in a shaker incubator at 200 rpm and the cell densities were determined at interval of one hour by the absorbance at 600 nm.

2.5. Cell viability measurement: The reduced number in viable cells treated with NPs was determined by CFU counting. After 1 ml cells and 100 µl samples were incubated at 37°C for 2 h, the mixture was serially (1:10) diluted. Subsequently, 100 µl cells suspension was spread onto an LB solid plate and left to grow at 37°C for 48 h. All assays were repeated three times. Colonies were counted and the survival rate was evaluated. The survival rate% = counts of samples treated with NPs/counts of control.

2.6. Detection of ROS levels: Oxidative stress generation is thought to be one of the key antibacterial mechanisms [28]. The intracellular ROS levels in the bacterial cells were determined, according to Guo *et al.* [29]. In brief, the cells were firstly mixed with Cu/PDA/RGO nanosheets in tubes (the control with DI water), and then the cells were washed with phosphate-buffered saline (PBS) solution and resuspended in PBS solution. Finally, 10 µl 2′,7′-dichlorofluorescein–diacetate was added and incubated for 1 h at room temperature in the dark. The fluorescence intensity was measured using an Edinburgh FLS920 spectrometer with excitation at 488 nm and emission at 525 nm.

2.7. Detection of integrity in cell membranes and morphological observation: Firstly, the cells were mixed with 200 µg/ml Cu/PDA/RGO nanosheets and incubated at 37°C for 2 h. Then, the supernatant was filtered through a 0.22 µm membrane, and the efflux of intracellular substances was measured by the absorbance at 260 nm. The morphological variations of bacteria were further investigated by scanning electron microscopy (SEM) examination. The collected cells are fixed using 2.5% glutaraldehyde overnight at 4°C, followed by dehydrating with a series of acetone solutions (10, 30, 50, 70, 90, and 100%). Finally, the cells were lyophilised and sputter-coated with gold for SEM observation.

3. Results and discussion

3.1. Characterisation studies: The XRD patterns of the as-obtained products are shown in Fig. 1*a*. For GO, a characteristic peak at 11.22°, corresponding to the (001) lattice plane, was observed. A reflection peak (002) at $2\theta = 26.2°$ appeared in the patterns of PDA/RGO and Cu/PDA/RGO nanosheets, indicating the successful reduction of GO to RGO by PDA [30]. However, the characteristic diffractions of Cu were not observed in the patterns of Cu/PDA/RGO, due to its low loading amount. Fig. 1*b* showed the TEM image of GO, in which the GO nanosheets exhibited a transparent lamellar structure with some wrinkles at the edges. In Fig. 1*c*, the surface of PDA/RGO appeared fairly rough, compared with that of GO. This result was consistent with the reduction of oxygen functional groups of GO and simultaneous coating of PDA on the surface of GO. The Cu clusters were not observed in the TEM image of Cu/PDA/RGO, probably due to low Cu loading (Fig. 1*d*).

XPS analysis determined the chemical composition of Cu/PDA/RGO nanosheets, as shown in Fig. 2. Fig. 2 shows the XPS survey spectrum of Cu/PDA/RGO. The peaks for C, O, N, and Cu were

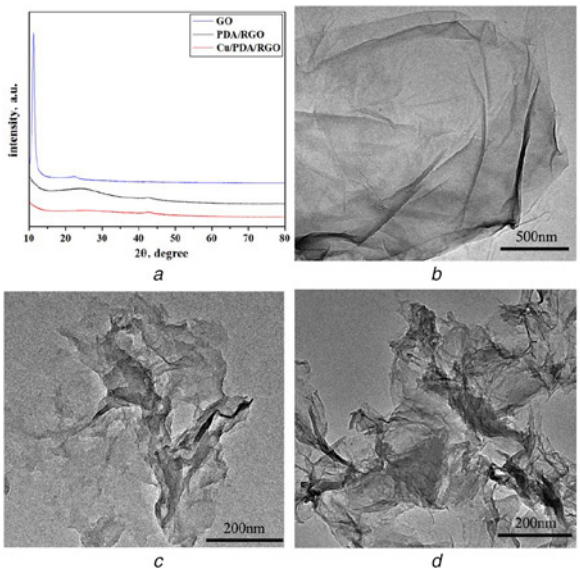

Fig. 1 *XRD patterns and TEM images of Cu/PDA/RGO nanosheets*
a XRD patterns of GO, PDA/RGO, and Cu/PDA/RGO nanosheets;
b TEM image of GO
c TEM image of PDA/RGO
d TEM image of Cu/PDA/RGO nanosheets

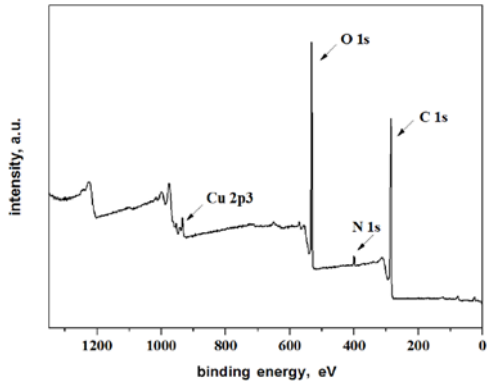

Fig. 2 *XPS survey spectrum of Cu/PDA/RGO*

observed, proving the presence of characteristic elements in Cu/PDA/RGO. As seen in the high-resolution scan (Fig. 3*a*), C 1s signal could be decomposed into four components: C=C (284.6 eV), C–N (285.2 eV), C–O (286.8 eV), and O–C=O (288.7 eV) [24]. Peaks with binding energies (BEs) at about 400.05 and 402.1 eV in Fig. 3*b* were attributed to the C–NH_2 and NH_3 species, respectively [31]. In the high-resolution scan of the O 1s (Fig. 3*c*), two peaks at 531.9 and 532.9 eV were observed, suggesting the presence of the PDA layer [32]. As seen in Fig. 3*d*, the characteristic peaks of Cu 2p at 934.7 eV and its corresponding satellite peak about 943.4 eV appeared, which suggested the presence of Cu^{2+} [2, 15]. The lower BE peak at 932.8 was assigned to Cu^{+} [33]. The concentration of Cu ions was further determined by ICP-OES, which was estimated to be 0.38 mg/kg.

3.2. Antibacterial studies: Cu NPs are known to exhibit antibacterial activity against many bacteria [3, 14]. In this study, *E. coli* and *S. aureus* cells were used for investigation of the antibacterial activity of the as-obtained products. The optical densities were determined and the growth curves were plotted, as shown in Figs. 4 and 5. The control samples showed rapid bacterial growth, and the delays in growth time of *E. coli* and *S. aureus* were 2 and 1 h, respectively (Figs. 4 and 5). Compared with control, as seen in Figs. 4*a* and *b*, GO and PDA/RGO did not inhibit the growth of *E. coli* cells at all tested concentrations. In contrast, the growth of *E. coli* cells was strongly inhibited by Cu/PDA/RGO nanosheets

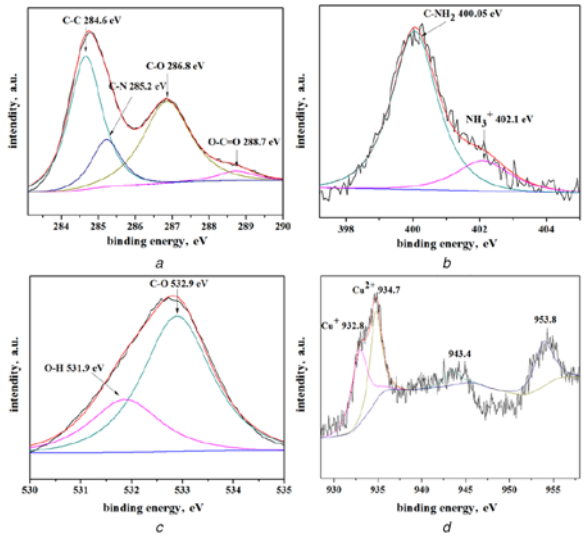

Fig. 3 *XPS spectra of Cu/PDA/RGO*
a C 1s
b N 1s
c O 1s
d Cu 2p

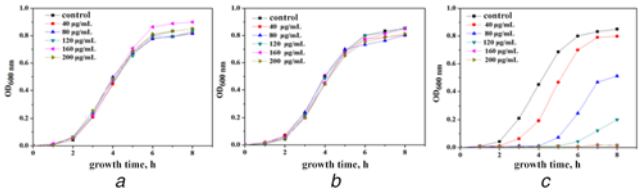

Fig. 4 *OD curves for growth of E. coli in LB broth at 37°C after the cell suspensions (2 ml, 10^7–10^8 cfu/ml) were treated with different concentrations of*
a GO
b PDA/RGO
c Cu/PDA/RGO nanosheets

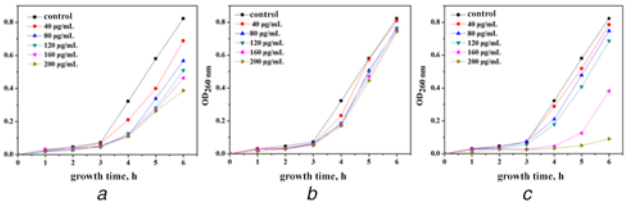

Fig. 5 *OD curves for growth of S. aureus in LB broth at 37°C after the cell suspensions (2 ml, 10^7–10^8 cfu/ml) were treated with different concentrations of*
a GO
b PDA/RGO
c Cu/PDA/RGO nanosheets

at concentrations of 80 µg/ml or more (Fig. 4*c*). The *E. coli* cells treated with 80 µg/ml nanosheets showed delay in their growth time by ∼4 h. For all nanosheet concentrations of >120 µg/ml the results obtained were same, showing delayed growth by >8 h (Fig. 4*c*). Figs. 5*a*–*c* show the antibacterial effects of samples on *S. aureus.* In Figs. 5*a* and *b*, GO and PDA/RGO hardly showed any delay in *S. aureus* growth, suggesting their weak antibacterial activities. The *S. aureus* cells treated with Cu/PDA/RGO nanosheet concentrations of below 120 µg/ml showed growth at a similar rate as that of the control blank (Fig. 5*c*). Nevertheless, the Cu/PDA/RGO nanosheets at concentrations of 160 and 200 µg/ml displayed excellent antibacterial efficiency, wherein the cell growth was delayed by ∼4 and 5 h, respectively (Fig. 5*c*).

To determine whether the as-obtained materials have a bactericidal effect on *E. coli* and *S. aureus* cells, cell viabilities were tested. As seen in Fig. 6, both bacteria had survival rates of about 100% in the presence of PDA/RGO, indicating no toxic effects of PDA/RGO on *E. coli* and *S. aureus* cells. Fig. 6*a* shows that there was no significant reduction in the number of viable *E. coli* cells in the presence of GO dispersion. Compared with other samples, the Cu/PDA/RGO nanosheets exhibited strong antibacterial activity against *E. coli*. As shown in Fig. 6*a*, the viable cell numbers were reduced by 26.5 and 49.1% after they were treated with Cu/PDA/RGO nanosheets at concentrations of 40 and 80 µg/ml, respectively. Moreover, treatments with concentrations of 120, 160, and 200 µg/ml could inactivate 93.3, 94.7, and 95.6% of viable *E. coli* cells, respectively (Fig. 6*a*). Fig. 6*b* shows the survival rates of *S. aureus* cells. Approximately 76–81% cells could survive when treated with different concentrations of GO (Fig. 6*b*), which suggested that the GO dispersions exhibited weak antibacterial performance. The Cu/PDA/RGO nanosheets at concentrations of 40, 80, and 120 µg/ml could inactivate 11.4–16.6% of the *S. aureus* cells (Fig. 6*b*). However, only 11.6 and 4.9% cells survived when treated with Cu/PDA/RGO nanosheets at concentrations of 160 and 200 µg/ml, respectively (Fig. 6*b*). These results clearly demonstrated enhanced antibacterial

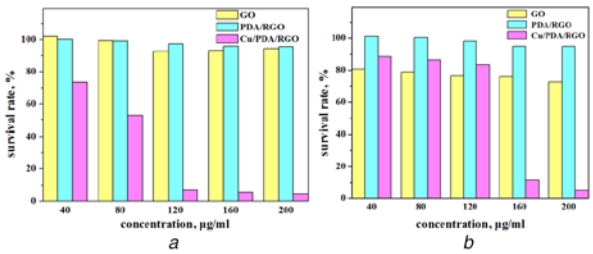

Fig. 6 *Survival rates of*
a E. coli cells
b S. aureus cells after incubation with different concentrations of GO, PDA/RGO, and Cu/PDA/RGO nanosheets for 2 h

doi: 10.1049/mnl.2019.0524

properties of Cu/PDA/RGO nanosheets. All these findings were consistent with the growth curves.

Results of bacterial viability tests showed that the Cu/PDA/RGO nanosheets had significant bactericidal activity against *E. coli* and *S. aureus*. To study the bactericidal mechanism, the accumulation of ROS was determined when cells were exposed to Cu/PDA/RGO nanosheets and the results are shown in Fig. 7. Compared with the blank control, the intracellular ROS levels of *E. coli* showed no apparent increase after treatment with Cu/PDA/RGO nanosheets at lower concentrations (40 and 80 µg/ml). However, the generation of ROS in *E. coli* cells had risen to 32.2, 41.5, and 65.2% when the concentrations of Cu/PDA/RGO nanosheets increased to 120, 160, and 200 µg/ml, respectively (Fig. 7*a*). In contrast, the ROS production in case of *S. aureus* was significantly higher after treatment with Cu/PDA/RGO nanosheets (Fig. 7*b*). Compared with control, the intracellular ROS levels showed a 1.6-fold increase at concentration of 40 µg/ml. Moreover, higher concentration of Cu/PDA/RGO nanosheets led to higher fluorescence intensity (Fig. 7*b*). Surprisingly, compared with control, Cu/PDA/RGO nanosheets with 200 µg/ml showed a 3.4-fold increase in ROS production (Fig. 7*b*). The significantly higher production of ROS by Cu/PDA/RGO nanosheets could play a major role in the antibacterial activity.

The UV–vis absorption assay was performed to further verify the integrity of the cell membrane. It is known that if the cell membrane of bacterium gets destroyed, the efflux of cytoplasmic materials, such as DNA and RNA, can change the absorbance intensity at 260 nm. The UV absorptivity at 260 nm is shown in Fig. 8 after the cells were incubated with Cu/PDA/RGO nanosheets and DI water. Compared with the control blank, the ratio of absorbance increased 2–5-fold with increase in concentration of Cu/PDA/RGO nanosheets (Fig. 8*a*). This indicated that *E. coli* cells were severely damaged and the intracellular substances had largely leaked out. In contrast, the ratio of *S. aureus* exhibited no remarkable changes before and after they were treated with Cu/PDA/RGO nanosheets (Fig. 8*b*), demonstrating that the cell membranes of *S. aureus* were not significantly affected by Cu/PDA/RGO

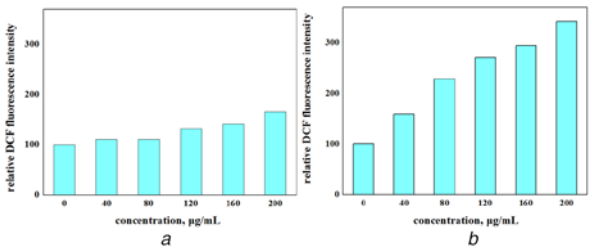

Fig. 7 *ROS generation after the*
a E. coli cells
b S. aureus cells were incubated with Cu/PDA/RGO nanosheets at different concentrations and DI water

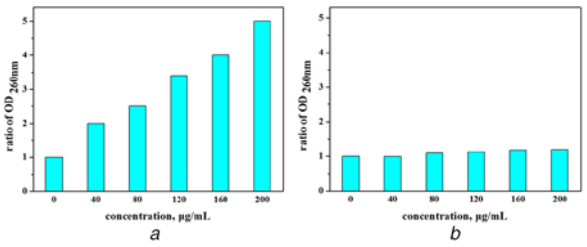

Fig. 8 *Absorbances of released cytoplasmic materials at 260 nm after*
a E. coli cells
b S. aureus cells were treated with different concentrations of Cu/PDA/RGO nanosheets

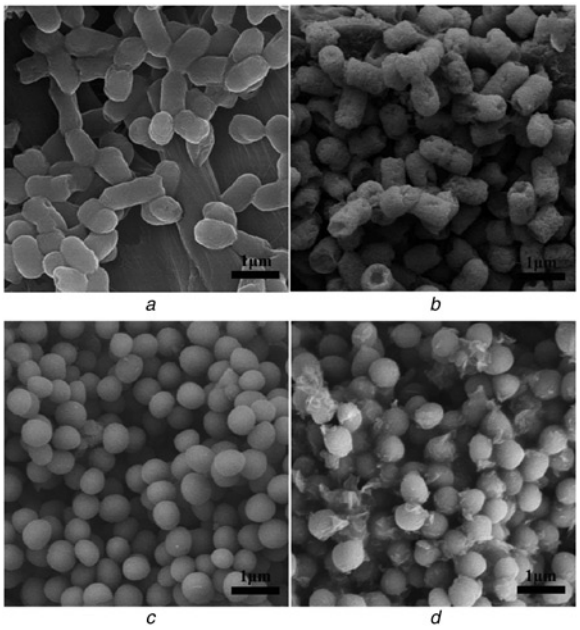

Fig. 9 *SEM images of E. coli and S. aureus treated with*
a, c Sterile DI water
b, d Cu/PDA/RGO (200 µg/ml)

nanosheets. It has been reported that the differences between antibacterial performances of carbon-based NPs are sometimes attributed to the bacterial cell structure [34]. In contrast to Gram-positive bacteria, the cells of Gram-negative bacteria have lipids in their external membranes. Carbon-based NPs readily enter through the lipid membrane. It is possible that the cytoplasmic materials are released due to the partitioning of Cu/PDA/RGO nanosheets into lipid membranes, leading to the death of *E. coli* cells. However, the Cu/PDA/RGO nanosheets do not seem to have impact on the cell membrane of *S. aureus*.

SEM was employed to further study the cell morphologies of samples treated with Cu/PDA/RGO nanosheets and the results are shown in Fig. 9. As seen in Fig. 9*a*, *E. coli* cells treated with DI water appeared rod-shaped with smooth and intact cell surfaces. In contrast, after treatment with Cu/PDA/RGO nanosheets, most *E. coli* cells became rough and porous with completely damaged cell walls (Fig. 9*b*). The antibacterial performance of Cu/PDA/RGO nanosheets could be attributed to the entry of Cu ions into the lipid cell membrane accompanied by the induction of more number of ROS species. This caused damage to the cell wall and leakage of cytoplasmic materials, which ultimately resulted in the death of *E. coli* cells [35, 36]. Fig. 9*c* shows the morphology of *S. aureus* cells, in which the blank control cells appeared spherical in shape with well-defined cell walls and smooth surfaces. The antibacterial efficiency of Cu/PDA/RGO nanosheets against *S. aureus* is shown in Fig. 9*d*. Although the surfaces of *S. aureus* remained intact, the Cu/PDA/RGO nanosheets were tightly wrapped around the cells (Fig. 9*d*). The antibacterial mechanism could possibly be attributed to the attachment of Cu ions to the cell wall, followed by generation of the active oxygen species due to the intracellular enzymes, causing cell death [9, 36].

4. Conclusions: In summary, highly efficient PDA/RGO nanosheets with incorporated Cu ions were synthesised using PDA as a reducing agent through a facile, efficient, and green method. Cu/PDA/RGO nanosheets exhibited better antibacterial performance against *E. coli* and *S. aureus*. The Cu ions could enter through the lipid membranes into the *E. coli* cells and induce the formation of higher ROS levels, damaging the cell membrane and causing leakage of cytoplasmic materials. This finally led

to the death of *E. coli* cells. On the other hand, the death of *S. aureus* could only be attributed to the production of high ROS levels, due to the direct contact with the samples. The facile fabrication and highly-efficient antibacterial ability of Cu/PDA/RGO nanosheets make them potential candidates for antibacterial nanomaterials.

5. Acknowledgments: We thank Hui Xia for the assistance with sample collection in the field. This research was supported by the Scientific Research Project in Colleges and Universities of Hebei Province (grant no. QN2019027), the Natural Science Foundation of Hebei Province (grant no. C2019407065), and the Program for the Top Young Talents of Higher Learning Institutions of Hebei Province (grant no. BJ2014026). Aiying Guo and Yanfeng Sun contributed equally to this work.

6 References

[1] Anand A., Unnikrishnan B., Wei S.C., *ET AL.*: 'Graphene oxide and carbon dots as broad-spectrum antimicrobial agents – a minireview', *Nanoscale Horiz.*, 2019, **4**, pp. 117–137

[2] Severino F., Brito J.L., Laine J., *ET AL.*: 'Nature of copper active sites in the carbon monoxide oxidation on $CuAl_2O_4$ and $CuCr_2O_4$ spinel type catalysts', *J. Catal.*, 1998, **177**, pp. 82–95

[3] Lewis K.: 'Platforms for antibiotic discovery', *Nat. Rev. Drug Discov.*, 2013, **12**, pp. 371–387

[4] Courtney C.M., Goodman S.M., McDaniel J.A., *ET AL.*: 'Photoexcited quantum dots for killing multidrug-resistant bacteria', *Nat. Mater.*, 2016, **15**, pp. 529–534

[5] Blair J M.., Webber M.A., Baylay A.J., *ET AL.*: 'Molecular mechanisms of antibiotic resistance', *Nat. Rev. Microbiol.*, 2015, **13**, pp. 42–51

[6] Szunerits S., Boukherroub R.: 'Antibacterial activity of graphene-based materials', *J. Mater. Chem. B*, 2016, **4**, pp. 6892–6912

[7] Burnham J.P., Lane M.A., Kollef M.H.: 'Impact of sepsis classification and multidrug-resistance status on outcome among patients treated with appropriate therapy', *Crit. Care Med.*, 2015, **43**, pp. 1580–1586

[8] Wang X.H., Han Q.S., Yu N., *ET AL.*: 'GO–AgCl/Ag nanocomposites with enhanced visible light-driven catalytic properties for antibacterial and biofilm-disrupting applications', *Colloids Surf. B, Biointerfaces*, 2018, **162**, pp. 296–305

[9] Farhoudian S., Yadollahi M., Namazi H.: 'Facile synthesis of antibacterial chitosan/CuO bio-nanocomposite hydrogel beads', *Int. J. Biol. Macromol.*, 2016, **82**, pp. 837–843

[10] Shen X.K., Hu Y., Xu G.Q., *ET AL.*: 'Regulation of the biological functions of osteoblasts and bone formation by Zn-incorporated coating on microrough titanium', *ACS Appl. Mater. Interfaces*, 2014, **6**, pp. 16426–16440

[11] Jadhav M.S., Kulkarni S., Raikar P., *ET AL.*: 'Green biosynthesis of CuO & Ag–CuO nanoparticles from malus domestica leaf extract and evaluation of antibacterial, antioxidant and DNA cleavage activities', *New J. Chem.*, 2018, **42**, pp. 204–213

[12] Dalecki A., Haeili M., Shah S., *ET AL.*: 'Disulfiram and copper ions kill mycobacterium tuberculosis in a synergistic manner', *Antimicrob. Agents Chemother.*, 2015, **59**, pp. 4835–4844

[13] Villanueva E., Maria Del Rosario Diez A., González J., *ET AL.*: 'Antimicrobial activity of starch hydrogel incorporated with copper nanoparticles', *ACS Appl. Mater. Interfaces*, 2016, **8**, pp. 16280–16288

[14] Chatterjee A., Kumar Sarkar R., Chattopadhyay A., *ET AL.*: 'A simple robust method for synthesis of metallic copper nanoparticles of high antibacterial potency against *E. coli*', *Nanotechnology*, 2012, **23**, p. 85103

[15] Bai H.W., Liu Z.Y., Sun D.: 'Hierarchical ZnO/Cu 'corn-like' materials with high photodegradation and antibacterial capability under visible light', *Phys. Chem. Chem. Phys.*, 2011, **13**, pp. 6205–6210

[16] Pang H., Wang S.M., Li G.C., *ET AL.*: 'Cu superstructures fabricated using tree leaves and Cu–MnO_2 superstructures for high performance supercapacitors', *J. Mater. Chem. A*, 2013, **1**, pp. 5053–5060

[17] Albadi J., Alihosseinzadeh A., Mansournezhad A., *ET AL.*: 'Novel metal oxide of CuO–ZnO nanocatalyst efficiently catalyzed the synthesis of 2-amino-4H-chromenes in water', *Synth. Commun.*, 2015, **45**, pp. 485–493

[18] Kiani F., Astani N., Tayyebi A., *ET AL.*: 'Effect of graphene oxide nanosheets on visible light-assisted antibacterial activity of vertically-aligned copper oxide nanowire arrays', *J. Colloid Interface Sci.*, 2018, **521**, pp. 119–131

[19] He W., Huang X. Q., Zheng Y. D., *ET AL.*: 'In situ synthesis of bacterial cellulose/copper nanoparticles composite membranes with long-term antibacterial property', *J. Biomater. Sci., Polym. Ed.*, 2018, **29**, pp. 1–29

[20] Nie N., He F., Zhang L.Y., *ET AL.*: 'Direct Z-scheme PDA-modified ZnO hierarchical microspheres with enhanced photocatalytic CO_2 reduction performance', *Appl. Surf. Sci.*, 2018, **457**, pp. 1096–1102

[21] Madhurakkat Perikamana Kumar S., Jinkyu L., Lee Y.B., *ET AL.*: 'Materials from mussel-inspired chemistry for cell and tissue engineering applications', *Biomacromolecules*, 2015, **16**, pp. 2541–2555

[22] Zhou Y., Li X., Wang Y.J., *ET AL.*: 'UV illumination enhanced molecular ammonia detection based on ternary reduced graphene oxide–titanium dioxide–Au composite film at room temperature', *Anal. Chem.*, 2019, **91**, pp. 3311–3318

[23] Kasprzak A., Poplawska M.: 'Recent developments in the synthesis and applications of graphene-family materials functionalized with cyclodextrins', *Chem. Commun.*, 2018, **54**, pp. 8547–8562

[24] Guo L.Q., Liu Q., Li G.L., *ET AL.*: 'A mussel-inspired polydopamine coating as a versatile platform for the in situ synthesis of graphene-based nanocomposites', *Nanoscale*, 2012, **4**, pp. 5864–5867

[25] Hu H.W., Xin J., Hu H.: 'Highly efficient graphene-based ternary composite catalyst with polydopamine layer and copper nanoparticles', *ChemPlusChem*, 2013, **78**, pp. 1483–1490

[26] Yeroslavsky G., Richman M., Dawidowicz L., *ET AL.*: 'Sonochemically produced polydopamine nanocapsules with selective antimicrobial activity', *Chem. Commun.*, 2013, **49**, pp. 5721–5723

[27] Wang X.P., Cai A.J., Wen X.L., *ET AL.*: 'Graphene oxide–Fe_3O_4 nanocomposites as high-performance antifungal agents against plasmopara viticola', *Sci. China Mater.*, 2017, **60**, pp. 258–268

[28] Li J.H., Zhou H.J., Wang J.X., *ET AL.*: 'Oxidative stress-mediated selective antimicrobial ability of nano-VO_2 against gram-positive bacteria for environmental and biomedical applications', *Nanoscale*, 2016, **8**, pp. 11907–11923

[29] Guo A.Y., Mu Q.Z., Cai A.J., *ET AL.*: 'Mussel-inspired green synthesis of Ag-coated polydopamine microspheres for selective antibacterial performance', *Micro Nano Lett.*, 2019, **14**, pp. 394–398

[30] Lian P.C., Zhu X.F., Liang S.Z., *ET AL.*: 'Large reversible capacity of high quality graphene sheets as an anode material for lithium-ion batteries', *Electrochim. Acta*, 2010, **55**, pp. 3909–3914

[31] Luo J., Jiang S.S., Liu X.Y.: 'Efficient one-pot synthesis of mussel-inspired molecularly imprinted polymer coated graphene for protein-specific recognition and fast separation', *J. Phys. Chem. C*, 2013, **117**, pp. 18448–18456

[32] Dong C., Wu K.L., Wei X.W., *ET AL.*: 'Synthesis of graphene oxide–Ag_2CO_3 composites with improved photoactivity and anti-photocorrosion', *Cryst. Eng. Commun.*, 2014, **16**, pp. 730–736

[33] Zhou S.G., Chen S.S., Yuan Y., *ET AL.*: 'Influence of humic acid complexation with metal ions on extracellular electron transfer activity', *Sci. Rep.*, 2015, **5**, p.17067

[34] Musico Y.F., Santos C.M., Dalida M.L., *ET AL.*: 'Surface modification of membrane filters using graphene and graphene oxide-based nanomaterials for bacterial inactivation and removal', *ACS Sustain. Chem. Eng.*, 2014, **2**, pp. 1559–1565

[35] Das D., Nath B., Phukon P., *ET AL.*: 'Synthesis and evaluation of antioxidant and antibacterial behavior of CuO nanoparticles', *Colloids Surf. B, Biointerfaces*, 2013, **101**, pp. 430–433

[36] Ingle A., Duran N., Rai M.: 'Bioactivity, mechanism of action, and cytotoxicity of copper-based nanoparticles: a review', *Appl. Microbiol. Biotechnol.*, 2014, **98**, pp. 1001–1009

doi: 10.1049/mnl.2019.0524